Growth of Mesoscale Ordered Two-Dimensional Hydrogen-Bond Organic Framework with the Observation of Flat Band

Minghu Pan, Xin Zhang, Yinong Zhou, Pengdong Wang, Qi Bian, Hang Liu, Xingyue Wang, Xiaoyin Li, Aixi Chen, Xiaoxu Lei, Shaojian Li, Zhengwang Cheng, Zhibin Shao, Haoxuan Ding, Jianzhi Gao, Fangsen Li, and Feng Liu

Phys. Rev. Lett. **130**, 036203 — Published 20 January 2023
DOI: 10.1103/PhysRevLett.130.036203

Growth of Mesoscale Ordered Two-dimensional Hydrogen-Bond Organic Framework with the Observation of Flat Band

Minghu Pan[1,2, #,*], Xin Zhang[3,#], Yinong Zhou[4,#], Pengdong Wang[5,#], Qi Bian [2], Hang Liu[4], Xingyue Wang[1], Xiaoyin Li[4], Aixi Chen[5], Xiaoxu Lei[5], Shaojian Li[2], Zhengwang Cheng[6], Zhibin Shao[1], Haoquan Ding[7], Jianzhi Gao[1,*], Fangsen Li[5,*] and Feng Liu[4,*]

[1]*School of Physics and Information Technology, Shaanxi Normal University, Xi'an 710119, China.*

[2]*School of Physics, Huazhong University of Science and Technology, Wuhan 430074, China.*

[3]*School of Physics, Northwest University, Xi'an, 710069, China.*

[4]*Department of Materials Science and Engineering, University of Utah, Salt Lake City, UT 84112, USA*

[5]*Vacuum Interconnected Nanotech Workstation, Suzhou Institute of Nano-Tech and Nano-Bionics, Chinese Academy of Sciences (CAS), Suzhou 215123, China*

[6]*School of Science and Hubei Engineering Technology Research Center of Energy Photoelectric Device and System, Hubei University of Technology, Wuhan 430068, China*

[7]*School of Physics and Astronomy, University of Birmingham, Birmingham, B15 2TT, United Kingdom.*

[#]These authors contributed equally to this work.

E-mail: minghupan@snnu.edu.cn; jianzhigao@snnu.edu.cn; fsli2015@sinano.ac.cn; fliu@eng.utah.edu

ABSTRACT

Flat bands (FBs), presenting a strongly interacting quantum system, have drawn increasing interest recently. However, experimental growth and synthesis of FB materials have been challenging and remained elusive for the ideal form of monolayer materials where the FB arises from destructive quantum interference as predicted in 2D lattice models. Here, we report surface growth of self-assembled monolayer of 2D hydrogen-bond (H-bond) organic frameworks (HOFs) of 1,3,5-tris(4-hydroxyphenyl)benzene (THPB) on Au(111) substrate and the observation of FB. High-resolution scanning tunneling microscopy/spectroscopy (STM/STS) shows mesoscale, highly-ordered and uniform THPB-HOF domains, while angle-resolved photoemission spectroscopy (ARPES) highlights a FB over the whole Brillouin zone (BZ). Density-functional-theory (DFT) calculations and analyses reveal that the observed topological FB arises from a hidden *electronic* breathing-Kagome lattice without *atomically* breathing bonds. Our findings demonstrate that self-assembly of HOFs provides a viable approach for synthesis of 2D organic topological materials, paving the way to explore many-body quantum states of topological FBs.

Introduction.— A topological FB presents an exotic Bloch state without band dispersion. It arises from destructive interference (phase cancelation) of Bloch wave functions, such as materials with a Kagome lattice [1-3] or more generally line-graph lattice models [1-9], differing from topologically trivial FBs of highly localized atomic orbitals, such as *f*-orbitals [10] and dangling bonds [11], and the FBs resulted from Moiré band folding of twisted bilayer graphene [12]. The phase cancelation renders the FB to be topological in both real space characterized with compact localized state [3] and momentum space having a singular touching point with a dispersive band [4,5]. Also, the completely quenched electron kinetic energy in a FB magnifies electron-electron interaction, leading to a range of theoretically predicted many-body quantum phases, such as fractional quantum Hall effect [7], Wigner crystallization [13], ferromagnetism [3,14], superconductivity [15] and excitonic insulator [16]. Recent discovery of superconductivity in twisted bilayer graphene has further boosted the interest in FBs [17].

On the other hand, various 2D FB-materials have been predicted from first-principles. These include 2D metalorganic frameworks (MOFs) [18-21], covalent organic frameworks (COFs) [14,22-25], HOF [26] and inorganic 2D materials [27]. Experimentally, FB features have been observed in the surface of transition-metal Kagome compounds [28-33], twisted bilayer graphene [34], and heterostructure [35], all having a layered structure which contains one atomic layer manifesting a 2D FB lattice model, such as Kagome lattice. But in these systems the FB is inevitably overlapping with many dispersive bands from other atomic layers. In general, experimental realization of topological FBs has been challenging due to lack of FB materials, especially elusive in the ideal form of monolayer materials originally proposed based on 2D lattice models. To date, there is no monolayer material that has been synthesized to enable direct observation of FB. A recent experiment has successfully grown COF monolayers of tribromotrioxaazatriangulene and tribromotrioxoazatriangulene on Au(111) substrate [36], enabling a clear observation of Dirac bands by ARPES; however, the FB, which was supposed to be present with a Kagome sublattice [36], cannot be directly observed because it is located ~1.0 eV above Fermi level [23].

In this Letter, we report direct observation of FB in a self-assembled monolayer of 2D HOF of THPB on Au(111) surface. Formation of mesoscale, uniform domains of THPB are seen by STM/STS, whose long-range order and lattice symmetry are further confirmed by low-energy electron diffraction (LEED). Remarkably, a FB over the whole BZ is observed by ARPES. Interestingly, DFT calculations reveal that the FB arises from a hidden *electronic* breathing-Kagome sublattice made of corner benzene rings (CBRs) of THPB, and hence topological non-trivial, but *atomically* all the CBRs locate at the sites of a Kagome lattice without breathing bonds. The electronic breathing effect is shown to be caused by different inter-CBR hopping mediated by H-bonds versus covalent bonds. Furthermore, the most salient features of H-bonds are characterized by high-resolution STM/STS, Raman spectroscopy and DFT calculations.

Experimental growth and structural characterization. — Instead of realizing FB-lattices using MOFs [14-17] and COFs [9,18,19] widely predicted by theory, we take a different approach to grow the less studied HOF, since H-bonds are weaker but more flexible than the organo-metallic and covalent bonds, in an attempt to assemble large-scale monolayer structures of high uniformity. We use THPB as a model molecule which are deposited onto Au(111) substrate at room temperature (see Methods in Supplemental Material (SM) [37] for sample preparation). The H-bond assisted self-assembly turns out to be very successful as evidenced in Fig. 1. We note that although synthesis and STM imaging of THPB-HOF has been reported before [58,59], those structures are mostly nanometer-sized islands, preventing them from ARPES measurement.

Figure 1a and 1b show large-scale STM images of 2D crystalline domains of THPB monolayer film at a coverage of 0.75 ML, where THPB molecules aggregate into a triangle lattice with long-range order. In Fig. 1b, the crystalline orientations of Au$[1\bar{1}0]$ and $[11\bar{2}]$ are determined by visualizing the well-known herringbone reconstruction of Au(111) surface [60]. Domain walls are observed with adjacent domains being mirror-symmetric with each other (Fig. S1 in SM [37]). The THPB-HOF lattices have been grown successfully over the entire substrate surface and remain intact across surface steps (see Fig. 1a and 1b).

High-resolution STM image (Fig. 1c) distinguishes each individual THPB molecule consisting of three bright protrusions from three CBRs, and reveals the self-assembled trigonal THPB lattice having a lattice constant of 14.6±0.2 Å. A schematic lattice model is drawn in Fig. 1d. The THPB molecules aggregate *via* formation of three H-bonds, rotated by 120° with each other, between the hydroxyl groups at the corner of THPB. The orientation of THPB-HOF lattice is determined whose lattice vectors a_1 (a_2) are aligned ~20° from the close-packed $[1\bar{1}0]$ direction of Au surface (see also Fig. S1c). Consequently, the BZ of HOF lattice and of Au(111) surface rotate away from each other by ~20°, as shown in Fig. 1e; the former is also ~5 times smaller than the latter. These relations are used for analyzing their respective ARPES spectra later.

The long-range order of THPB-HOF lattice is further confirmed by LEED, displaying diffraction spots from a periodic superstructure (Fig. 1g). It confirms the HOF domains are aligned in the same orientation, with a trigonal lattice rotated by 20° from that of the Au(111) surface (Fig. 1f). The lattice constant of HOF is extracted to be ~1.5 nm from LEED, in very good agreement with STM. These findings demonstrate that epitaxial growth of 2D HOFs offers a viable approach to synthesize organic 2D materials, especially monolayer HOFs with desirable electronic properties, such as the FB as demonstrated below.

ARPES observation of flat band. — Importantly, the mesoscale size and mono-orientation of 2D THPB-HOF has enabled characterization of its band structure by ARPES, which has been used to investigate band structure of other organic systems [61-63]. As a reference, the ARPES of bare Au(111) surface was measured first (Fig. 2a). The well-known Shockley surface states with a parabolic valley at -0.5 eV are observed. In addition, the parabolic Au surface *sp* band having the bottom of valley at ~ -3.6 eV and some bulk bands lying at the lower energies are also visible, in agreement with previous reports [64,65]. The *d* band of Au locates below −3.8 eV.

We have grown 2D THPB-HOFs from ~0.5 monolayer (ML) to nearly-full coverage on

Au(111) surface with their long-range order all confirmed by STM and LEED. Figure 2b shows the ARPES measured from one of the 0.5 ML samples, along the K_{Au}-Γ-K_{Au} direction of the Au(111) BZ. Remarkably, a FB is seen at the energy of -2.62 eV (see also the second-derivative intensity plot in the middle panel). The Au Shockley surface state is no longer visible upon molecular coverage, while its *sp* surface bands and bulk *d* bands become weaker. The FB gives rise to a distinct peak in the density of state (DOS) (right) which is absent in the DOS of bare Au (Fig. 2a). Considering Au-HOF forming a metal-semiconductor heterojunction and assuming the Fermi level of Au is aligned with the mid-gap position of HOF, the position of FB at -2.62 eV sets a lower limit for the bandgap of HOF to be 5.24 eV (see band diagram in Fig. S2 [37]). The other DOS peaks in the right panel of Fig. 2b, *e.g.* -3.9 eV, are aligned well with the top/bottom of some parabolic bands from Au *sp* and bulk states.

To confirm the FB exists in the whole 2D BZ, we conducted also low-temperature ARPES measurement at 12 K on a sample of nearly-full coverage of THPB-HOF. The constant-energy contour (CEC) at -2.67 eV is shown in Fig. 3a, which signifies the presence of the circular Au *sp* band appearing near the BZ boundary. Furthermore, to reveal the truly flatness of FB, three line-cuts are taken along momentum paths of Γ-K_{HOF}, Γ-K_{Au} and M_{HOF}-Γ-M_{HOF}, as indicated by yellow dashed lines in Fig. 3a. The cut 1 (Fig. 3b) and 2 (Fig. 3c) are taken with the energies from -2.2 to -3.4 eV. Both intensity (left) and second-derivative (right) plots of cut 1 and 2, show a FB (band 1) at -2.62 eV, indicating it touches with a weakly dispersive band (band 2) at the Γ point, as the theory would predict (dashed lines). There is also a parabolic Au surface *sp* band intersects with these two HOF bands. Two entangled bands can be distinguished more clearly in the spectrum of cut 3 (Fig. 3d), and interestingly, a third strongly dispersive band shows up below the above-mentioned two bands. This third band is further confirmed by the energy distribution curves (EDC) measured from -0.39 to 0.39 Å^{-1} (Fig. 3e). By deconvoluting these three bands, the FB energy is resolved at -2.57 eV, slightly different from its apparent position of -2.62 eV in Fig. 2b. Overall, the band dispersions are clearer in Fig. 3d than those in Fig. 3b and 3c, partly because the cut 3 is outside the circular Au *sp* band at the BZ boundary (Fig. 3a), so that the Au *sp* band sits above without overlapping with the FB. More line-cut spectra are available in Fig. S3 [37].

Topological FBs from a hidden breathing-Kagome sublattice. —The THPB-HOF has an apparent triangle lattice, as shown in Fig. 1d, which is not expected to host FB. To reveal the origin of the observed FB, we have performed DFT calculations. The optimized lattice structure and the calculated band structure are shown in Fig. 4a and 4b, respectively. The THPB-HOF is a semiconductor having a FB below the Fermi level as the VBM (Fig. 4b), consistent with the experiment (Fig. 2b and S2 [37]). We note that the calculated gap of ~ 3.0 eV from local-density-approximation (LDA) is corrected to ~4.0 eV by Heyd-Scuseria-Ernzerhof (HSE) functional, which is still ~ 1.0 eV smaller than the experimental value in Fig. 2b. This is reasonable considering there could be some charge transfer from Au surface to HOF to shift the Fermi level of HOF above its mid-gap position and the HSE gap may still be an underestimation [66]. We also did calculation using van der Waals functional (DFT-D2) to better treat H-bonds, which did not show significant difference.

Figure 4b shows that the FB touches with a dispersive band below, as observed. A checkerboard lattice could have such a two-band configuration [67], but the THPB-HOF lattice does not have a square lattice symmetry. So, also the lower lying dispersive band, observed in ARPES as well (band 3 in Fig. 3d), has to be considered in the analysis. This led us to realize that it resembles the typical three-bands structure of a breathing-Kagome lattice, consistent with the trigonal lattice symmetry of HOF [68]. However, a closer inspection of lattice structure (Fig. 4a) finds a perfect Kagome lattice with two identical size of triangles within the unit cell; while a breathing-Kagome lattice has two triangles of different size, as if one breathes outward and the other inward (Fig. 4c) [68]. To resolve this inconsistency, we plot the charge density of the designated three bands overlaid on the lattice in Fig. 4a, which are mainly contributed by C and O p_z orbitals (Fig. S6 [37]). Then, we uncovered that a sublattice of effectively breathing-Kagome type is formed by three CBRs of THPB molecules *via* two different inter-CBR hopping, namely the H-bonds mediated by O/H atoms versus the covalent bonds mediated by the center benzene ring in THPB. Consequently, an interesting scenario of “a breathing-Kagome lattice without breathing" is materialized, with the effect of breathing achieved *electronically* by different lattice hopping strength *via* H-bond (t_H) and covalent bond (t_C) for the same bond length, as indicated in Fig. 4a and illustrated in Fig. 4c.

To further confirm the above identification of FB, we have fit the three DFT-LDA bands of interest with a tight-binding (TB) breathing-Kagome lattice Hamiltonian, as shown in Fig. 4d. One sees that the TB bands (red dotted lines) agree well with the DFT bands (blue solid lines) using two fitting parameters of t_H = 0.05 eV and t_C = 0.26 eV, and the former is much smaller than the latter indicating a strong electronic breathing effect. The fact that the experimentally observed FB is flat over the whole BZ with a singular touching point with a dispersive band indicates it is topological nontrivial [4,5]. In contrast, trivial FB of localized molecular orbitals is usually not flat over the whole BZ and/or isolated without a singular band touching point. This is further supported by a good agreement between the observed bands with theoretical bands whose topological properties are directly calculated. Using the TB model, we calculated the compact localized state and noncontractible loop state in real space to illustrate nontrivial FB topology, which is also confirmed by calculation of topological invariant in *k*-space (Fig. S6 [37]). Moreover, we made Wannier fitting of the DFT-LDA bands (cyan dotted lines in Fig. 4d), and simulated the ARPES spectra (see Methods and Fig. S7 [37]). The Wannier band dispersions along three paths, Γ to K_{HOF}, Γ to K_{Au} and M_{HOF}-Γ_{HOF}-M_{HOF} are calculated as black dashed lines overlaid on the experimental spectra in Fig. 3b-3d, respectively. Note that we used DFT-LDA results for fitting the three breathing-Kagome bands because their band dispersions agree better than HSE bands with experiments after aligning the positions of FB. Qualitatively, either LDA or HSE bands confirm the origin of FB from a breathing-Kagome lattice.

Further experimental evidence of H-bond and breathing Kagome lattice. —To better resolve the H-bond, we performed differential conductance (dI/dV) mapping along with STM imaging, to visualize the local charge DOS. Figure 4e and 4f shows the topographic STM image and the dI/dV image, respectively. One sees that the local DOS of covalent C-C bonds bridging the

CBRs within a THBP molecule is much higher than that of H-bonds bridging the CBRs in between the THBP molecules. This again indicates that the sublattice of all CBRs forms an effective breathing-Kagome hopping pattern, as the intra-THBP CBR-CBR hopping (t_C in Fig. 4f) *via* covalent bonds is much stronger than the inter-THBP CBR-CBR hopping (t_H in Fig. 4f) *via* H-bonds, although the intra-THBP CBR-CBR distance (d_C = 7.4 Å) is about the same as the inter-THBP CBR-CBR distance (d_H = 7.2 Å), as show in Fig. 4e. This confirms an *electronic* breathing-Kagome lattice without *atomic* breathing bonds. Additional evidence for H-bonds is collected from *in-situ* Raman spectroscopic measurement (Fig. S4 [37]), supported by DFT phonon calculations (Fig. S9 [37]).

Conclusion. —We demonstrate successful growth of self-assembled mesoscale, highly-ordered and uniform monolayer THPB-HOF films, which has enabled observation of a topological FB. DFT calculations reveal the FB to be originated from a hidden *electronic* breathing-Kagome lattice without *atomic* breathing bonds. Our findings pave the way to future realization of 2D topological and FB materials by the demonstrated approach of self-assembly of HOFs, for which a wide range of molecular precursors and substrates can be explored.

Acknowledgements. —M. H. Pan, X. Zhang and F. S. Li acknowledge financial support from the National Natural Science Foundation of China (11574095, 91745115, 22102129 and 11634007). Y. N. Zhou, X. Y. Li and F. Liu acknowledge financial support from DOE-BES (No. DE-FG02-04ER46148). F. S. Li also acknowledge financial support from the Suzhou Science and Technology Program (Grant No. SJC2021009) and the Youth Innovation Promotion Association of Chinese Academy of Sciences (2017370). Sample growth, Raman and ARPES measurements were conducted at the Vacuum Interconnected Nano-X Research Facility in SINANO, Suzhou. STM work was conducted at School of Physics, Huazhong University of Science and Technology in Wuhan. The calculation was done on the CHPC at the University of Utah and US-DOE-NERSC.

References

[1] A. Mielke, Ferromagnetism in the Hubbard model on line graphs and further considerations, J. Phys. A: Math. Gen. **24**, 3311 (1991)

[2] A. Mielke, Ferromagnetic ground-states for the Hubbard-model on line graphs, J. Phys. A: Math. Gen. **24**, L73 (1991).

[3] Z. Liu, F. Liu, and Y.-S. Wu, Exotic electronic states in the world of flat bands: From theory to material, Chin. Phys. B **23**, 077308 (2014).

[4] D. L. Bergman, C. Wu, and L. Balents, Band touching from real-space topology in frustrated hopping models, Phys. Rev. B **78** (2008).

[5] J.-W. Rhim and B.-J. Yang, Classification of flat bands according to the band-crossing singularity of Bloch wave functions, Phys. Rev. B **99** (2019).

[6] J. Ma, J. W. Rhim, L. Tang, S. Xia, H. Wang, X. Zheng, S. Xia, D. Song, Y. Hu, Y. Li, B. J. Yang, D. Leykam, and Z. Chen, Direct Observation of flatband loop states arising from nontrivial real-space topology, Phys. Rev. Lett. **124**, 183901 (2020).

[7] E. Tang, J. W. Mei, and X. G. Wen, High-temperature fractional quantum Hall states, Phys. Rev. Lett. **106**, 236802 (2011).

[8] H. Liu, G. Sethi, S. Meng, and F. Liu, Orbital design of flat bands in non-line-graph lattices via line-graph wave functions, Phys. Rev. B **105** (2022).

[9] D. Călugăru, A. Chew, L. Elcoro, Y. Xu, N. Regnault, Z.-D. Song, and B. A. Bernevig, General construction and topological classification of crystalline flat bands, Nat. Phys. **18**, 185 (2022).

[10] G. R. Stewart, Non-Fermi-liquid behavior in *d*- and *f*-electron metals, Rev. Mod. Phys. **73**, 797 (2001).

[11] D. Yu, E. M. Lupton, H. J. Gao, C. Zhang, and F. Liu, A unified geometric rule for designing nanomagnetism in graphene, Nano Res. **1**, 497 (2008).

[12] R. Bistritzer and A. H. MacDonald, Moire bands in twisted double-layer graphene, Proc. Natl. Acad. Sci. USA **108**, 12233 (2011).

[13] C. Wu, D. Bergman, L. Balents, and S. Das Sarma, Flat bands and Wigner crystallization in the honeycomb optical lattice, Phys. Rev. Lett. **99**, 070401 (2007).

[14] W. Jiang, H. Huang, and F. Liu, A Lieb-like lattice in a covalent-organic framework and its Stoner ferromagnetism, Nat. Commun. **10**, 2207 (2019).

[15] S. Miyahara, S. Kusuta, and N. Furukawa, BCS theory on a flat band lattice, Physica C Supercond. **460-462**, 1145 (2007).

[16] G. Sethi, Y. Zhou, L. Zhu, L. Yang, and F. Liu, Flat-band-enabled triplet excitonic Insulator in a diatomic kagome lattice, Phys. Rev. Lett. **126**, 196403 (2021).

[17] Y. Cao, V. Fatemi, S. Fang, K. Watanabe, T. Taniguchi, E. Kaxiras, and P. Jarillo-Herrero, Unconventional superconductivity in magic-angle graphene superlattices, Nature **556**, 43 (2018).

[18] Z. Liu, Z.-F. Wang, J.-W. Mei, Y.-S. Wu, and F. Liu, 20 Flat Chern Band in a Two-Dimensional Organometallic Framework, Phys. Rev. Lett. **110** (2013).

[19] Z. F. Wang, N. Su, and F. Liu, 21 Prediction of a two-dimensional organic topological insulator, Nano Lett. **13**, 2842 (2013).

[20] T. Kambe, R. Sakamoto, T. Kusamoto, T. Pal, N. Fukui, K. Hoshiko, T. Shimojima, Z.

Wang, T. Hirahara, K. Ishizaka, S. Hasegawa, F. Liu, and H. Nishihara, Redox control and high conductivity of nickel bis(dithiolene) complex pi-nanosheet: a potential organic two-dimensional topological insulator, J. Am. Chem. Soc **136**, 14357 (2014).

[21] W. Wang, N. Ni, and F. Liu, Exotic topological bands and quantum states in meta organic and covalent-organic frameworks, Acc. Chem. Res. **54**, 416 (2021).

[22] B. Cui, X. Zheng, J. Wang, D. Liu, S. Xie, and B. Huang, Realization of Lieb lattice in covalent-organic frameworks with tunable topology and magnetism, Nat. Commun. **11**, 66 (2020).

[23] X. Ni, H. Li, F. Liu, and J. L. Bredas, Engineering of flat bands and Dirac bands in two-dimensional covalent organic frameworks (COFs): relationships among molecular orbital symmetry, lattice symmetry, and electronic-structure characteristics, Mater. Horiz. **9**, 88 (2022).

[24] Y. Jing and T. Heine, Making 2D topological polymers a reality, Nat. Mater. **19**, 823 (2020).

[25] S. Ghosh, Y. Tsutsui, T. Kawaguchi, W. Matsuda, S. Nagano, K. Suzuki, H. Kaji, and S. Seki, Band-like transport of charge carriers in oriented two-dimensional Conjugated covalent organic frameworks, Chem. Mater. **34**, 736 (2022).

[26] C.-H. Liu, A. Wei, M. F. Cheung, and D. F. Perepichka, Vanishing electronic band gap in two-dimensional hydrogen-bonded organic frameworks, Chem. Mater. **34**, 3461 (2022).

[27] H. Liu, S. Meng, and F. Liu, Screening two-dimensional materials with topological flat bands, Phys. Rev. Mater. **5** (2021).

[28] Z. Lin, J. H. Choi, Q. Zhang, W. Qin, S. Yi, P. Wang, L. Li, Y. Wang, H. Zhang, Z. Sun, L. Wei, S. Zhang, T. Guo, Q. Lu, J. H. Cho, C. Zeng, and Z. Zhang, Flatbands and emergent ferromagnetic ordering in Fe_3Sn_2 kagome lattices, Phys. Rev. Lett. **121**, 096401 (2018).

[29] Q. W. T. Y. Yang, Y. H. Wang, M. Song, J. Tang, Z. W. Wang, H. Z. Lv, N. C. Plumb, M. Radovic, G. W. Wang, G. Y. Wang, Z. Sun, R. Yu, M. Shi, Y. M. Xiong, N. Xu, Evidence of orbit-selective electronic Kagome lattice with planar flat-band in correlated paramagnetic YCr_6Ge_6, arXiv preprint arXiv: 1906.07140 (2019).

[30] Z. Liu, M. Li, Q. Wang, G. Wang, C. Wen, K. Jiang, X. Lu, S. Yan, Y. Huang, D. Shen, J. X. Yin, Z. Wang, Z. Yin, H. Lei, and S. Wang, Orbital-selective Dirac fermions and extremely flat bands in frustrated kagome-lattice metal CoSn, Nat. Commun. **11**, 4002 (2020).

[31] M. Kang, S. Fang, L. Ye, H. C. Po, J. Denlinger, C. Jozwiak, A. Bostwick, E. Rotenberg, E. Kaxiras, J. G. Checkelsky, and R. Comin, Topological flat bands in frustrated kagome lattice CoSn, Nat. Commun. **11**, 4004 (2020).

[32] M. Li, Q. Wang, G. Wang, Z. Yuan, W. Song, R. Lou, Z. Liu, Y. Huang, Z. Liu, H. Lei, Z. Yin, and S. Wang, Dirac cone, flat band and saddle point in kagome magnet YMn_6Sn_6, Nat. Commun. **12**, 3129 (2021).

[33] M. Kang, L. Ye, S. Fang, J. S. You, A. Levitan, M. Han, J. I. Facio, C. Jozwiak, A. Bostwick, E. Rotenberg, M. K. Chan, R. D. McDonald, D. Graf, K. Kaznatcheev, E. Vescovo, D. C. Bell, E. Kaxiras, J. van den Brink, M. Richter, M. Prasad Ghimire, J. G. Checkelsky, and R. Comin, Dirac fermions and flat bands in the ideal kagome metal

FeSn, Nat. Mater. **19**, 163 (2020).

[34] S. Lisi, X. B. Lu, T. Benschop, T. A. de Jong, P. Stepanov, J. R. Duran, F. Margot, I. Cucchi, E. Cappelli, A. Hunter, A. Tamai, V. Kandyba, A. Giampietri, A. Barinov, J. Jobst, V. Stalman, M. Leeuwenhoek, K. Watanabe, T. Taniguchi, L. Rademaker, S. J. van der Molen, M. P. Allan, D. K. Efetov, and F. Baumberger, Observation of flat bands in twisted bilayer graphene, Nat. Phys. **17**, 189 (2021).

[35] T. Yilmaz, X. Tong, Z. Dai, J. T. Sadowski, E. F. Schwier, K. Shimada, S. Hwang, K. Kisslinger, K. Kaznatcheev, E. Vescovo, and B. Sinkovic, Emergent flat band electronic structure in a VSe_2/Bi_2Se_3 heterostructure, Commun. Mater. **2** (2021).

[36] G. Galeotti, F. De Marchi, E. Hamzehpoor, O. MacLean, M. Rajeswara Rao, Y. Chen, L. V. Besteiro, D. Dettmann, L. Ferrari, F. Frezza, P. M. Sheverdyaeva, R. Liu, A. K. Kundu, P. Moras, M. Ebrahimi, M. C. Gallagher, F. Rosei, D. F. Perepichka, and G. Contini, Synthesis of mesoscale ordered two-dimensional pi-conjugated polymers with semiconducting properties, Nat. Mater. **19**, 874 (2020).

[37] See Supplemental Material at http://link.aps.org/... for supplemental text, Figs. S1–S10, which includes Refs. [38–57].

[38] I. Horcas, R. Fernandez, J. M. Gomez-Rodriguez, J. Colchero, J. Gomez-Herrero, and A. M. Baro, WSXM: a software for scanning probe microscopy and a tool for nanotechnology, Rev. Sci. Instrum. **78**, 013705 (2007).

[39] J. P. Perdew and A. Zunger, Self-interaction correction to density-functional approximations for many-electron systems, Phys. Rev. B **23**, 5048 (1981).

[40] G. E. S. a. M. E. Jochen Heyd, Erratum: "Hybrid functionals based on a screened Coulomb potential" [J. Chem. Phys. 118, 8207 (2003)], J. Chem. Phys. **122**, 234102 (2005).

[41] J. Paier, M. Marsman, and G. Kresse, Why does the B3LYP hybrid functional fail for metals?, J. Chem. Phys. **127**, 024103 (2007).

[42] G. Kresse and J. Furthmuller, Efficient iterative schemes for ab initio total-energy calculations using a plane-wave basis set, Phys. Rev. B **54**, 11169 (1996).

[43] M. Methfessel and A. T. Paxton, High-precision sampling for Brillouin-zone integration in metals, Phys. Rev. B **40**, 3616 (1989).

[44] D. Hobbs, G. Kresse, and J. Hafner, Fully unconstrained noncollinear magnetism within the projector augmented-wave method, Phys. Rev. B **62**, 11556 (2000).

[45] Q. Wu, S. Zhang, H.-F. Song, M. Troyer, and A. A. Soluyanov, WannierTools: An open-source software package for novel topological materials, Comput. Phys. Comm. **224**, 405 (2018).

[46] N. Marzari and D. Vanderbilt, Maximally localized generalized Wannier functions for composite energy bands, Phys. Rev. B **56**, 12847 (1997).

[47] A. Farrell, A. Arsenault, and T. Pereg-Barnea, Dirac cones, Floquet side bands, and theory of time-resolved angle-resolved photoemission, Phys. Rev. B **94** (2016).

[48] M. A. Sentef, M. Claassen, A. F. Kemper, B. Moritz, T. Oka, J. K. Freericks, and T. P. Devereaux, S11 Theory of Floquet band formation and local pseudospin textures in pump-probe photoemission of graphene, Nat. Commun. **6**, 7047 (2015).

[49] J. K. Freericks, H. R. Krishnamurthy, and T. Pruschke, Theoretical description of time-resolved photoemission spectroscopy: application to pump-probe experiments, Phys.

Rev. Lett. **102**, 136401 (2009).

[50] N. Koch *et al.*, Energy levels at interfaces between metals and conjugated organic molecules, *J. Phys.: Condens. Matter* **20**, 184008(2008).

[51] A. Franco-Canellas *et al.*, Binding and electronic level alignment of pi-conjugated systems on metals, *Rep. Prog. Phys.* **83**, 066501(2020).

[52] Y. Ling, W. C. Xie, G. K. Liu, R. W. Yan, Y. Wu, and J. Tang, The discovery of the hydrogen bond from p-Nitrothiophenol by Raman spectroscopy: Guideline for the thioalcohol molecule recognition tool, Sci. Rep. **6**, 31981 (2016).

[53] Z. Lin, J. H. Choi, Q. Zhang, W. Qin, S. Yi, P. Wang, L. Li, Y. Wang, H. Zhang, Z. Sun, L. Wei, S. Zhang, T. Guo, Q. Lu, J. H. Cho, C. Zeng, and Z. Zhang, Flatbands and emergent ferromagnetic ordering in Fe_3Sn_2 kagome lattices, Phys. Rev. Lett. **121**, 096401 (2018).

[54] T. Korzdorfer *et al.* When to trust photoelectron spectra from Kohn-Sham eigenvalues: The case of organic semiconductors, Phys. Rev. B **79**, 201205, 2009.

[55] A. Haags *et al.*, Momentum space imaging of pi orbitals for chemical analysis, Sci. Adv. **8**, eabn0819 (2022)

[56] M. Preuss and F. Bechstedt, Vibrational spectra of ammonia, benzene, and benzene adsorbed on Si(001) by first principlescalculations with periodic boundary conditions, Phys. Rev. B **73** (2006).

[57] L. D. Ziegler and B. Hudson, Resonance Raman scattering of benzene and benzene□d6 with 212.8 nm excitation, J. Chem. Phys. **74**, 982 (1981)

[58] A. C. Marele, I. Corral, P. Sanz, R. Mas-Ballesté, F. Zamora, M. Yáñez, and J. M. Gómez-Rodríguez, Some pictures of alcoholic dancing: from simple to complex hydrogen-bonded networks based on polyalcohols, J. Phys. Chem. C **117**, 4680 (2013).

[59] Q. Li, B. Yang, H. Lin, N. Aghdassi, K. Miao, J. Zhang, H. Zhang, Y. Li, S. Duhm, J. Fan, and L. Chi, Surface-controlled mono/diselective ortho C-H bond activation, J. Am. Chem. Soc. **138**, 2809 (2016).

[60] C. Woll, S. Chiang, R. J. Wilson, and P. H. Lippel, Determination of atom positions at stacking-fault dislocations on Au(111) by scanning tunneling microscopy, Phys. Rev. B **39**, 7988 (1989).

[61] G. Koller *et al.*, Intra- and Intermolecular Band Dispersion in an Organic Crystal, Science **317**, 351 (2007).

[62] S. Ciuchi *et al.*, Molecular Fingerprints in the Electronic Properties of Crystalline Organic Semiconductors: From Experiment to Theory, Phys. Rev. Lett. **108**, 256401 (2012).

[63] Y. Nakayama *et al.*, Photoelectron spectroscopy on single crystals of organic semiconductors: experimental electronic band structure for optoelectronic properties, J. Mater. Chem. C, **8**, 9090(2020).

[64] A. Winkelmann, C. Tusche, A. Akin Ünal, M. Ellguth, J. Henk, and J. Kirschner, Analysis of the electronic structure of copper via two-dimensional photoelectron momentum distribution patterns, New J. Phys. **14**, 043009 (2012).

[65] P. M. Sheverdyaeva, R. Requist, P. Moras, S. K. Mahatha, M. Papagno, L. Ferrari, E. Tosatti, and C. Carbone, Energy-momentum mapping ofd-derived Au(111) states in a thin film, Phys. Rev. B **93** (2016).

[66] A. J. Garza and G. E. Scuseria, Predicting band gaps with hybrid density functionals, J. Phys. Chem. Lett. **7**, 4165 (2016).

[67] K. Sun, Z. Gu, H. Katsura, and S. Das Sarma, Nearly flatbands with nontrivial topology, Phys. Rev. Lett. **106**, 236803 (2011).

[68] M. Ezawa, Higher-order topological insulators and semimetals on the breathing kagome and pyrochlore lattices, Phys. Rev. Lett. **120**, 026801 (2018).

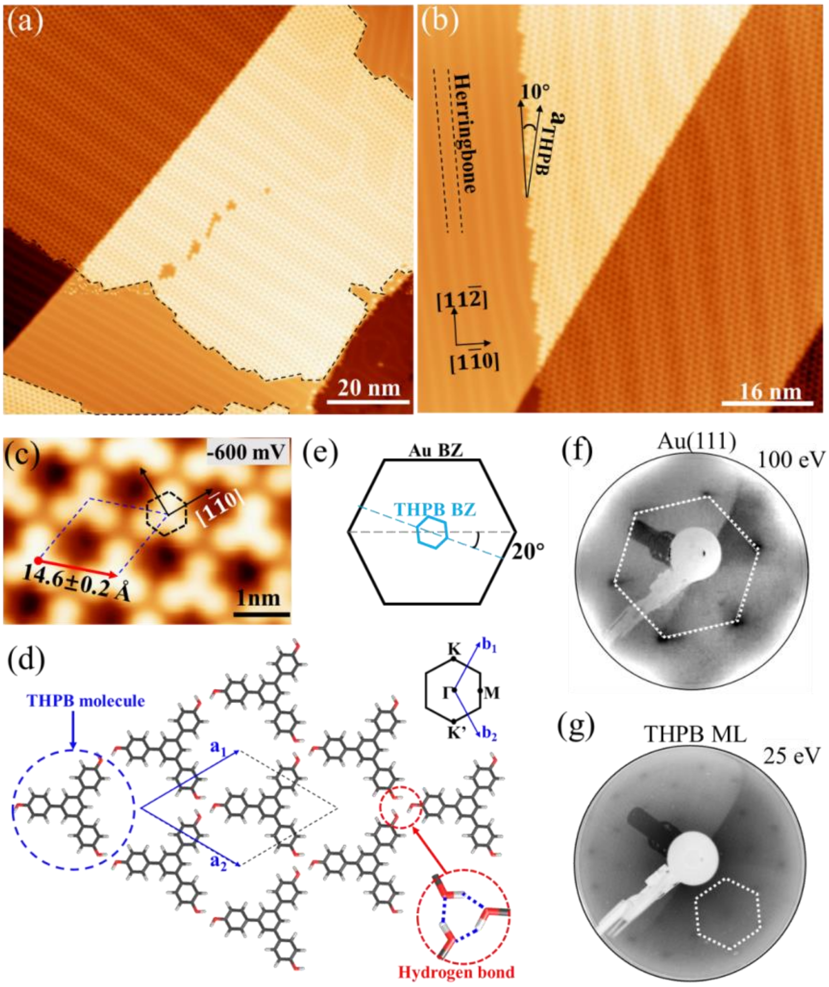

Fig. 1. (a) and (b) Large-scale topographic STM images (I_t = 200 pA, V_b = -0.5 V). The orientation of HOF is determined whose lattice vector is aligned ~10º away from the Au-$[11\bar{2}]$

direction. (c) Close-up STM image showing a trigonal lattice with a lattice constant of 14.6±0.2 Å, averaged from line profiles. The dashed hexagon marks the unit cell of Au lattice showing the close-packed $[1\bar{1}0]$ direction which has a 20° angle with the THPB-HOF lattice vectors. (d) Schematic lattice model indicating three H-bonds in between THPB. (e) The relationship between the BZ of Au(111) surface and of HOF. (f) and (g) LEED patterns of clean and HOF-covered Au(111) surface taken at the energies of 100 eV and 25 eV, respectively. Their reciprocal lattices are marked with white dashed hexagons.

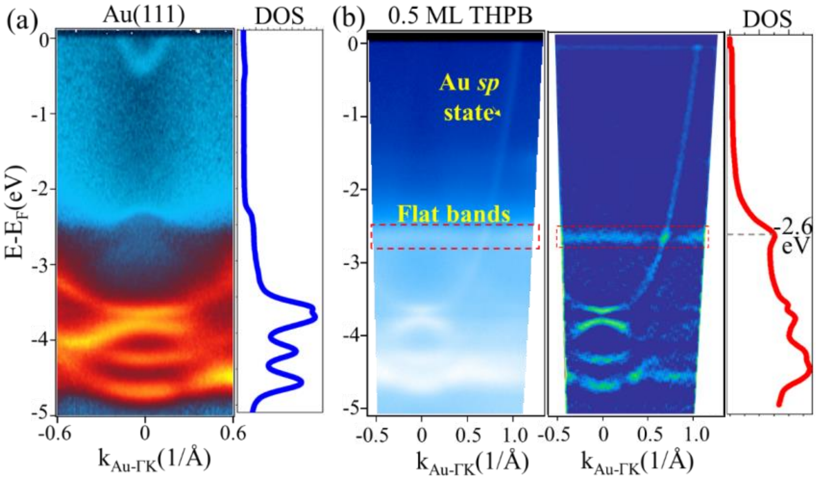

Fig. 2. (a) The photoemission intensity plot of E_B-k_x cut along the K_{Au}-Γ-K_{Au} direction at $k_y=0$ (left) and the integrated DOS from ARPES (right), taken from the bare Au(111) surface. K_{Au} is the K point of Au(111) surface BZ. (b) The ARPES spectra (left), the second-derivative plot (middle), and the integrated DOS from the ARPES showing a peak at the FB energy of -2.62 eV (right), taken along Γ-K_{Au} direction from a 0.5-monolayer THPB film.

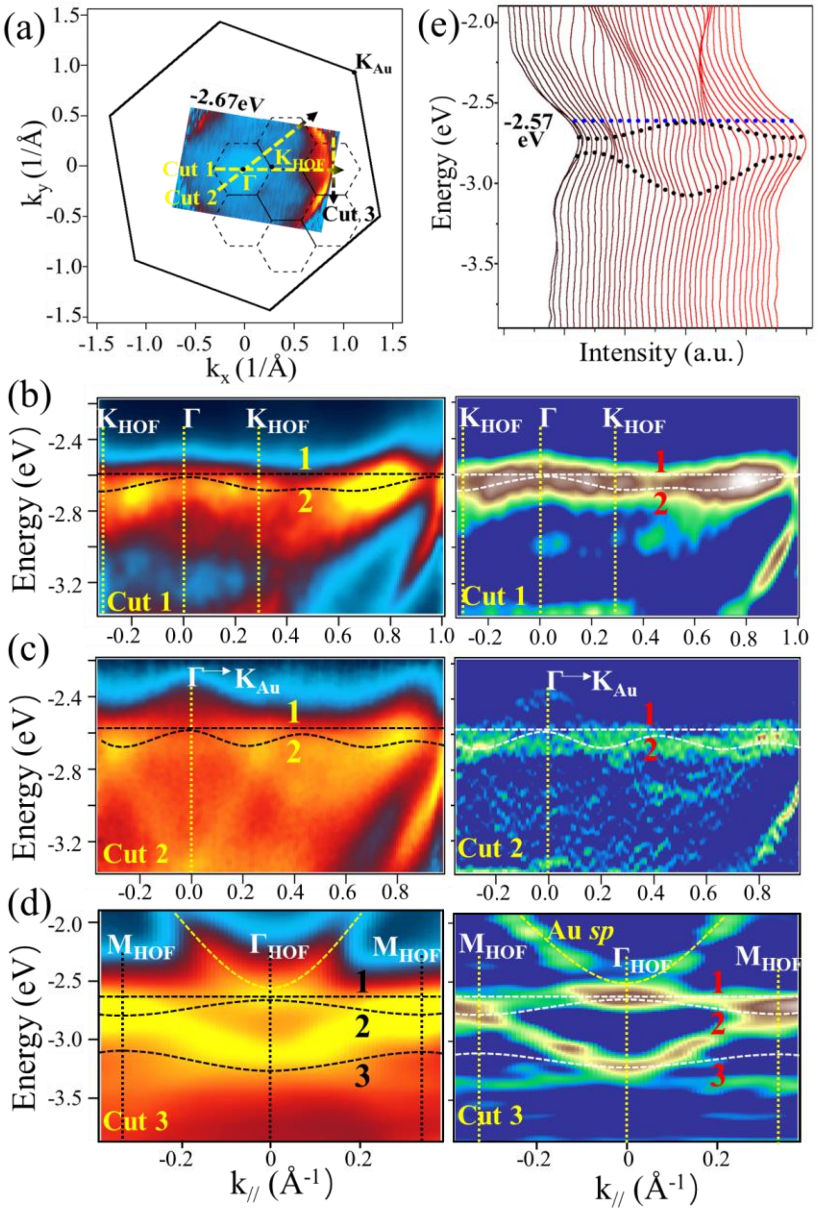

Fig.3. (a) The CEC measured at -2.67 eV and 12 K. The states of Au *sp* bands is clearly visible near the BZ boundary (half circle). The yellow dashed lines indicate three line-cuts taken for ARPES measurements in (b) - (d). (b) High-resolution ARPES (left) and second-derivative (right) plots measured at 12 K from cut 1 along the Γ-K$_{HOF}$ direction as marked in (a). (c) Same

Commented [FL1]: This figure may not fit in one-column anymore. I suggest to place (a) and (e) parallel on top, then (b),(c) and (d) at bottom, to fit.

as (b) for cut 2 along Γ-K_{au}. (d) Same as (b) for cut 3 along M_{HOF}-Γ_{HOF}-M_{HOF}. K_{HOF}, Γ_{HOF} and M_{HOF} are special *k*-points in the BZ of THPB-HOF. The dashed black lines are the DFT-LDA-Wannier bands superimposed on the experimental spectra. (e) The EDC of (d). The blue/black dotted lines denote the peak positions obtained by Gaussian fitting, representing band 1, 2 and 3. The FB (band 1) locates at -2.57 eV.

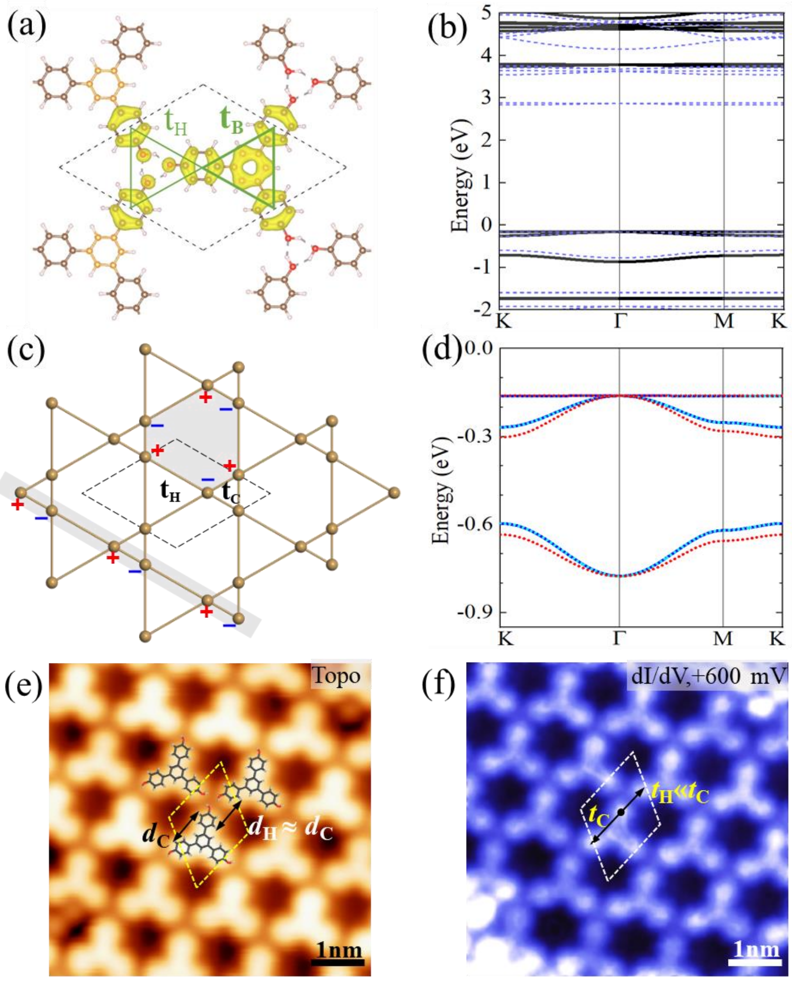

Fig. 4. (a) The optimized lattice structure ovelaid with partial charge density derived from the top three valence bands belonging to the breathing-Kagome lattice formed by CBRs of THPB. The brown/orange, red and pink balls represent C, O and H atoms, respectively. The charge

density is plotted using an isosurface of 0.002 eV/Å^3. (b) The LDA band structure (blue dashed lines) with a gap corrected by HSE functional (black solid lines). (c) Illustration of an electronic breathing-Kagome lattice formed by different hopping strength of t_H *via* H-bonds vs. t_C via covalent bonds (see also Fig. 4a), as if there were breathing bonds of different lengths. (d) The fit of the top three DFT valence bands (blue solid lines) by the TB breathing-Kagome lattice model (red dotted lines) and Wannier bases (cyan dotted lines). (e) Topographic STM image and (f) differential conductance (dI/dV) mapping taken simutaniously at +600 meV, using V_B= -200 mV, I_T= 300 pA and a bias modulation of 5 mV.